ELSEVIER

Contents lists available at ScienceDirect

Applied Surface Science

journal homepage: www.elsevier.com/locate/apsusc



Full Length Article

An investigation of the interaction and pH-activity relationship of ceria nanoparticles with a model membrane

Natalia Domenech-Garcia ^{a,b}, Nicole Hondow ^b, Andrew Nelson ^{a,*}, Rik Drummond-Brydson ^b

ARTICLE INFO

Keywords: Rapid cyclic voltammetry Model membrane Ceria nanoparticles Nanoparticle toxicity Membrane interaction

ABSTRACT

Using rapid cyclic voltammetry (RCV) and an established electrochemical sensor, we clarify the interactions of in-house synthesised and well characterised cerium (IV) oxide (ceria) nanoparticles and nanocubes (NPs) with phospholipid membranes. The RCV results reveal that the interaction of ceria NPs with the phospholipid depends not only on the dispersion media and the particle coating, but also on the pH. No interaction was observed with the phospholipid layer when ceria NPs were dispersed in phosphate buffered saline (PBS) at pH 7.4 or in citric acid/citrate buffers (CCB) at pH values \geq 4. However, a clear interaction was observed when ceria NPs were dispersed in acidic media. Notably, CeO₂ NPs dispersed in either a glycine buffer at pH 3.0 (GLY 3.0) or CCB at pH 3.0, when in contact with the phospholipid monolayer, exhibited similar interaction behaviours to soluble Ce (+III) ions dispersed in the same media. However, both RCV responses also showed an increase in the background current (a semiconductor effect) indicative of the direct interaction of the nanoparticles with the uncoated electrode. In contrast, PBS-incubated ceria NPs did not produce an interaction with the phospholipid monolayer when dispersed in CCB 3.0 or GLY 3.0. Together, these findings suggest that the dispersion medium plays an important role in the interaction of CeO₂ NPs either impeding or promoting interaction by changing the characteristics of the NP surface. In particular, we conclude that the interaction of ceria NPs with the phospholipid layer at acidic pH is facilitated by Ce(+III) ions or their complexes on the surface of the nanoparticles.

1. Introduction

The use of nanoparticles (NPs) is becoming increasingly popular in technological applications due to their enhanced and often size-dependent functions and properties [1–5]. However, the increase in nanoparticle production and use may result in a potential increase in their direct exposure to living organisms [6]. In addition, other indirectly synthesised NPs, generated as a secondary product of different processes, can be released into the environment and interact with their surroundings [7,8]. For this reason, NP toxicity testing is becoming increasingly important. Traditional toxicity tests analyse the dose–response relationship between a certain compound (e.g. a chemical or a nanoparticle in an appropriate medium) and a cell culture or whole organism. However, the complexity of the testing system does not easily permit the identification of the key properties of the NPs affecting their interaction behaviour. Potentially this interaction can depend not only on their direct physico-chemical properties such as particle size, shape,

surface chemical composition and the presence (or absence) of any surface coating, but also on additional properties, such as the concentration of NPs and the dispersion medium, as well as the surface charge and agglomeration state.

In this work, we simplify this challenge via use of rapid cyclic voltammetry (RCV) within a well-controlled environment. The membrane activity of CeO_2 NPs is investigated by measuring their direct interaction with a phospholipid monolayer using an electrochemical sensor, previously developed by Nelson [9], that mimics a cell membrane (see section 2.4 for a detailed justification). This has been previously used to assess the toxicity of organic molecules in water [10] indicating similar interactions (indicative of toxicity) to those observed during *in vitro* tests [11]. In addition, it has been previously used to assess the interaction of nanoparticles such as SiO_2 [12], ZnO [13] or titanium dioxide TiO_2 NPs [14] with phospholipids. This technique, unlike traditional toxicity testing, can provide fundamental information on the exact nature of the interaction between the nanoparticle and the model membrane. The

E-mail address: a.l.nelson@leeds.ac.uk (A. Nelson).

a School of Chemistry, The University of Leeds, Leeds LS2 9JT, UK

^b School of Chemical and Process Engineering, The University of Leeds, Leeds LS2 9JT, UK

^{*} Corresponding author.

RCV response primarily consists of two capacitance current peaks that are related to the phase transitions occurring in the phospholipid layer on the liquid mercury electrode as a function of applied voltage [15]. Upon interaction of species with the phospholipids, a suppression or shift of the capacitance current peaks is observed, which is specific to the type of interaction [16].

Cerium (IV) oxide, CeO2, is traditionally known for being a highly refractory, insoluble material. CeO2 NPs are widely used in a broad range of fields from the automobile industry to pharmacy. They are commonly used as an oxygen buffer or as a catalyst in redox reactions. This is due to the ability of CeO2 NPs to change between +IV and +III oxidation states under certain conditions and thereby act as an oxygen scavenger or source [17,18]. Upon reduction, oxygen vacancies are generated to maintain the neutrality and reduce the structural tension of the unit cell [19]. This ability is utilised, for example, in three-way catalysts (TWC) to help to transform toxic exhaust fumes (hydrocarbons, CO and NO_x) produced during hydrocarbon combustion to less harmful gases such as H₂O, CO₂ and N₂ [20-22], as well as in diesel engines to reduce soot combustion [23] and in solid oxide fuel cells (SOFCs) [24]. In addition, cerium based materials are used in water splitting [25,26] and in water waste treatment [27] due to their photocatalytic properties.

Furthermore, in recent years, CeO_2 NPs have expanded into the biomedical field. The oxygen storage capacity of ceria is used to produce or control reactive oxygen and nitrogen species and it has been used as an anti-inflammation agent [28], in cancer therapy [29], as an anti-obesity drug [30] or to repair bones and to influence neuronal growth [31].

However, there are many contradictory reports about the potential toxicity of CeO_2 NPs. On one side of the debate, there are those who contend that CeO_2 NPs have a biologically protective effect. In general, they suggest that the presence of Ce^{3+} , and thus oxygen vacancies on the particle surface, could allow reactive oxygen species (ROS) to be scavenged. This would result in a decrease of oxidative stress, similar to the effect of the superoxide dismutase (SOD) or catalase enzymes in biological environments [32–37]. Conversely, there are those who propose an oxidase enzyme-like activity of CeO_2 NPs with some studies suggesting that CeO_2 NPs produce oxidative stress that can lead to apoptosis and cell death [38–41].

This paper attempts to clarify the activity mechanisms through which CeO₂ NP dispersions interact with a model membrane monolayer by means of RCV. The effects of particle size, pH, dispersion media and coatings have been analysed.

2. Materials and methods

2.1. Materials

Cerium (III) nitrate hexahydrate (99.99 %), 1 M tetramethylammonium hydroxide (TMAOH) ACS reagent, hexamethylenetetramine (HMT) ACS reagent (\geq 99 %), phosphate buffered saline (PBS), pH 7.4 (powder) ACS reagent (>99 %), citric acid monohydrate ACS reagent (\geq 99 %), sodium citrate tribasic dihydrate (\geq 99.5 %) and potassium chloride ACS grade, were purchased from Sigma Aldrich. Glycine-HCl buffer, 10 mM, pH 3.0 was obtained from Bio-Rad. 1,2-dioleoyl-sn-glycero-3-phosphocholine (DOPC) was purchased from Avanti Polar Lipids. Milli-Q water (Millipore, UK) with a resistivity of 18.2M Ω -cm and a total organic carbon content of 4 ppb was used during all experiments.

2.2. Synthesis methods

Highly dispersed spherical ceria nanoparticles are commercially available (from e.g. Alfa Aesar or Sigma Aldrich). However, they invariably exhibit an unknown coating (possibly citrate) which could alter the interaction with the electrochemical sensor and, as a result,

samples were instead synthesised in house (however, for completeness the dataset from such commercial nanoparticles are given in section S1 of the Supplementary Information). Thus, two different types of CeO_2 NPs were synthesised using wet chemical methods. Both syntheses used $Ce(NO_3)_3 \cdot 6H_2O$ as a precursor and TMAOH or HMT respectively. The synthesis procedures for CeO_2 NPs were based on a personal communication with the 'Catalan Institute of Nanoscience and Nanotechnology' (ICN2) [42]. In this work CeO_2 NPs synthesised using TMAOH are referred to as 'spheres', while CeO_2 NPs synthesised using HMT are referred to as 'cubes'.

Spheres were synthesised by mixing 37.5 mM of $Ce(NO_3)_3 \cdot 6H_2O$ with 40 mM TMAOH in milli-Q water, dropwise and under continuous stirring at room temperature for 48 h. The dispersion was centrifuged and the obtained powder was cleaned by resuspension and further centrifugation in milli-Q water three times before use. Subsequently, the cleaned CeO_2 NPs were air-dried at room temperature overnight before use.

Cubes were synthesised using 37.5 mM of $Ce(NO_3)_3 \cdot 6H_2O$ and 0.5 M HMT in milli-Q water. The solution of $Ce(NO_3)_3 \cdot 6H_2O$ was poured into HMT under continuous stirring. The resulting solution was stirred in a closed bottle at room temperature for 48 h. The pellet was cleaned three times by resuspension and centrifugation using milli-Q water. Subsequently, the pellet was air-dried overnight at room temperature before use.

Finally, in order to investigate further the effects of NP morphology, additionally ceria nanoneedles were synthesised via a hydrothermal route. However, it was observed that these invariably broke on ultrasonication, and hence, we de-prioritised their study. However, for completeness, we summarise the dataset in section S2 of the Supplementary Information (SI).

2.2.1. Sample preparation

 CeO_2 NP dispersions were prepared by dispersing the dried powders obtained from the syntheses at a concentration of 0.01 M (of ceria NPs and, hence, cerium ions) in three different buffers. Phosphate buffered saline (pH 7.4) and glycine buffer (pH 3.0) were commercially purchased and are referred to as PBS and GLY, respectively. The pKa values of glycine are pKa₁ = 2.4 (ionisation of the carboxyl group in positively charged glycinium to a zwitterion) and pKa₂ = 9.7 (ionisation of the ammonium cation in the zwitterion to negatively charged glycinate) [43].

In addition, CeO_2 NPs were also dispersed in citric acid/ citrate buffers (CCB). Four different CCB buffers were prepared by mixing the appropriate amounts of citric acid monohydrate and tri-sodium citrate dihydrate to obtain pH values of 3.0 (CCB 3.0), 4.0 (CCB 4.0), 5.0 (CCB 5.0) and 6.0 (CCB 6.0), respectively. The pH values of the buffers were measured three times prior to the experiments. The pKa values of the carboxyl groups in citric acid are pKa₁ = 3.1, pKa₂ = 4.8 and pKa₃ = 6.4 at 25 °C [44].

2.3. Characterisation methods

2.3.1. Morphology and structural characterisation

Bright-field transmission electron microscopy (BFTEM) images and selected area electron diffraction (SAED) patterns were obtained by using a FEI Tecnai F20 field emission gun TEM operated at 200 kV and equipped with a Gatan Orius SC600A charge-coupled device (CCD) camera. Electron energy loss EELS (EELS) were obtained using an FEI Titan Themis 300 operated at 300 kV and equipped with a Gatan Quantum ER energy filter and Gatan OneView 4 K CMOS digital camera. In both cases, TEM samples were prepared by drop casting a dispersion of nanoparticles (if appropriate in the dispersion medium involved) onto a holey carbon-support film on copper, 300 mesh grids purchased from Agar Scientific. Average particle sizes were obtained by measuring over 300 particles. In addition, a Bruker D8 X-ray diffractometer, using Cu K α radiation at 40 mA, 45 kV was used to obtain the X-Ray diffraction data from the bulk powders.

2.3.2. Characterisation of nanoparticle dispersions

A Zetasizer nano ZSP particle size analyser from Malvern instruments was used to assess the stability of the NP dispersions. Dynamic light scattering (DLS) was used to assess the agglomeration state of the NPs in the different media and, in addition, surface charges on the particles were measured using Zeta Potential (ZP) analysis. Uncoated CeO $_2$ NPs present high polydispersity indices and aggregate with time. Thus, CeO $_2$ NPs were sonicated for 30 min and were then left to rest 5 min before carrying out the DLS measurements, in order to match the experimental conditions used in the electrochemical measurements.

2.3.3. Dissolution behaviour

Inductively coupled plasma mass spectrometry (ICP-MS) (Perkin Elmer, Elan DRCe) was used to study the amount of dissolved cerium (+III) in the dispersions. The method described in [45] was used to prepare the samples for ICP-MS. This method ensures the removal of any nanoparticulate matter prior to analysis which means that the Ce detected is all associated with either free ions or complexes of Ce (+III). In order to replicate the experimental conditions used in the electrochemical measurements, 0.01 M of the spheres/cubes were dispersed in CCB 3.0, GLY 3.0 and PBS 7.4 via sonication for 30 min. Subsequently, the samples were centrifuged at 14,000 rpm for 30 min and the dispersion media was separated from the pellet. Then, any remaining nanoparticles in the supernatant (which could give false positive results) were separated by passing through a Vivacon ultrafiltration spin column equipped with a Hydrosart cellulose membrane of 2 kDa molecular weight cut-off (equating to an approximately 1.5 nm pore size) from Sartorius. Following a dilution of 100 times (0.1 mL of the supernatant diluted in 10 mL of the desired buffer), the concentration of cerium (ug L^{-1}) in the supernatant was measured using ICP-MS in to identify the amount of dissolved cerium from the ceria NPs. A cerium ICP-MS standard (elemental cerium in 2 % HNO3 (1000 $\mu g/mL$) from SPEX Certi-Prep) was used to create calibration curves for each of the different media (from 10 ppm to 10 ppt).

2.4. Rapid cyclic voltammetry measurements (RCV)

Rapid cyclic voltammetry was used to measure the interaction between a model phospholipid membrane and the CeO_2 NPs. A schematic diagram of the electrochemical testing system is shown in Fig. 1. It consists of a flow cell with electrodes directly connected to a PGSTAT12 potentiostat (Autolab, Metrohm) and interfaced to a computer. In addition, the cell is connected to a buffer reservoir. The flow cell contains eight micro-fabricated platinum working electrodes, on which liquid mercury is deposited (hereafter referred to as Hg/Pt), two platinum auxiliary electrodes and an Ag/AgCl reference electrode [9]. In addition, the buffer is connected to a continuous source of Argon gas to eliminate oxygen from the solution [10].

Phospholipid monolayers, such as DOPC, can be deposited on the Hg/Pt electrode by cycles of fluctuating potential as described below. The hydrophobicity of the phospholipid tails and the Hg facilitate their adsorption [46]. The adsorption of the phospholipid on the Hg/Pt

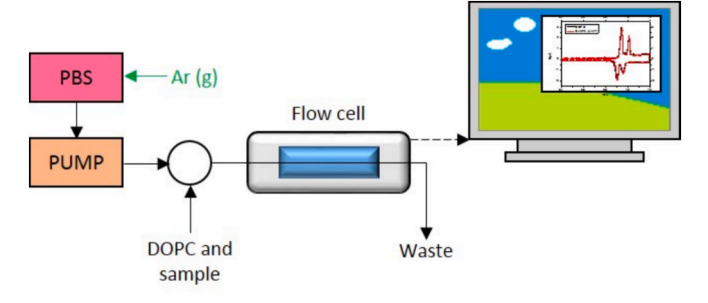


Fig. 1. Schematic diagram of the RCV device.

creates a dynamic system [46] which mimics half a lipid bilayer. At a certain potential, phospholipids re-arrange to form different phases [15] and these phase changes are observed as current peaks in the voltammograms [15,47,48]. When any substance, dissolved or particulate, interacts with the phospholipid, it can cause a variation in the intermolecular forces within the layer. These variations are represented as a suppression or a shift of the current peaks of the RCV. This is a fingerprint which indicates how the NPs and the phospholipid interact [47]. An in-depth explanation of the technique can be found in [9,10,15,47,48].

In the development of a successful pre-screening toxicity platform, one has to maintain a balance between a technology which is robust, reproducible, both rapid and routine for use and one which is relevant to biological *in vitro* cell toxicity measurements. The biomembrane sensor applied in this paper represents such a system and has been shown in several intercalibrations with other vesicle [49,50] and *in vitro* [51,52] technologies to be sensitive to biomembrane active particles and solutes. The reason for this is that the fluid phospholipid (DOPC) is a realistic representation of the fluid phospholipid component of cell membranes which depends on this fluidity for their function. Hence, any disruption of this fluidity when the phospholipid interacts with particles/compounds as recorded by the described biomembrane sensor will affect the function of all biomembrane components of ion channels and enzymes as well as affecting biomembrane permeability.

Analyses of the various dispersions were carried out according to the following procedure:

- Ar(g) was flowed through the buffer for 30 min to eliminate dissolved oxygen.
- 2. The flow rate of the buffer was set to be constant at 4.67 mL s $^{-1}$.
- 3. The Hg/Pt electrode was cleaned by applying potential cycles from -0.4~V to -1.2~V at a scan rate of $100~V~s^{-1}$ for 5 min.
- 4. Phospholipid deposition: 1 mL of oxygen-free DOPC in milli-Q water (2 mg mL⁻¹) was initially de-oxygenated with Ar(g) for 15 min and then introduced into the system whilst applying potential cycles from −0.4 V to −3.0 V at a scan rate of 100 V s⁻¹. Two current peaks, characteristic of the DOPC monolayer, then appeared and the potential was stopped. Subsequently, potential cycles from −0.4 V to −1.2 V at a scan rate of 40 V s⁻¹ were applied resulting in the characteristic DOPC voltammogram. Note, it has been shown in earlier studies that the scan rate of 100 V s⁻¹ of voltage excursion −0.4 to −3 V was necessary to rapidly open the vesicles in the DOPC dispersion, so allowing the phospholipid to spread on the electrode surface [9]. On the other hand, a scan rate of 40 V s⁻¹ of range −0.4 to −1.2 V is sufficient for measuring the capacitance of the spread monolayer. Higher scan rates lead to an apparent broadening and depression of the capacitance peaks.
- 5. The potential was then set to $-0.4\,\mbox{V}$ and the buffer flow was stopped.
- 6. Sample testing: the NP dispersions were sonicated for 30 min prior to testing and any oxygen was eliminated from the dispersions by flowing through Ar(g) for 5 min. Subsequently, 1 mL of the sample dispersion was introduced into the system. Then, potential cycles from -0.4~V to -1.2~V at a scan rate of $40~V~s^{-1}$ were applied and after 5 s the flow was switched on.

3. Results and discussion

3.1. Nanoparticle characterisation

3.1.1. Size, shape and crystalline structure

As observed in Fig. 2, the synthesised NPs consisted of spheres of 4.28 \pm 0.28 nm diameter (Fig. 2a and b) and cubes of 10.57 \pm 0.17 nm on a side (Fig. 2d and e), both exhibited log-normal size distributions. Additional TEM images of both samples, at a range of different magnifications which more clearly reveal the morphologies and single crystalline nature of the particles are included in the supplementary

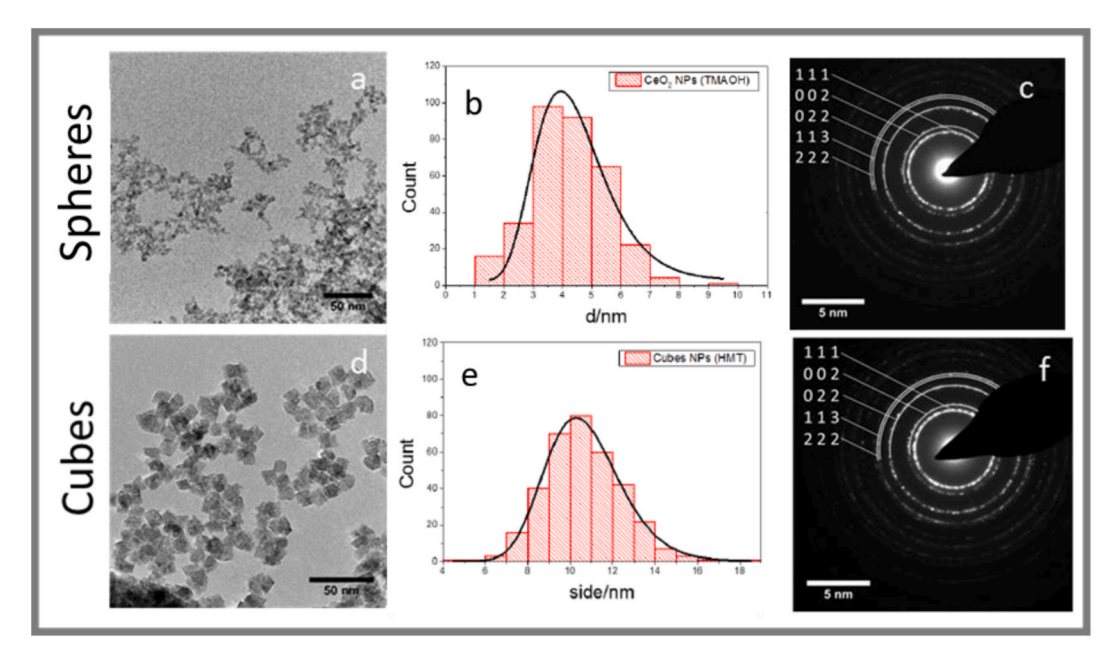


Fig. 2. (a) BFTEM image of CeO₂ NPs synthesised using TMAOH in water. (b) Size distribution curve of the NPs synthesised with TMAOH. (c) SAED pattern of the NPs synthesised with TMAOH. (d) BFTEM image of CeO₂ NPs synthesised using HMT. (e) Size distribution curve of the NPs synthesised with HMT in water. (f) SAED pattern of the NPs synthesised with HMT.

information (SI) in section S3, Figs. S3.1.1 and S3.1.2. Energy Dispersive X-ray analysis in the TEM showed the presence of only cerium and oxygen (see SI section S3, Fig. S3.2). Indexed SAED patterns (Fig. 2c and f) confirmed that they were pure CeO_2 NPs according to ICDD file: 00-004-0593 with a crystalline cubic structure (Fm-3m) and unit cell parameters a=b=c=5.4110 Å. This was supported by the XRD patterns that are included in the SI in section S3, Fig. S3.3.

3.1.2. Dispersion characteristics

Assessing the agglomeration state of nanoparticles within dispersions using solely TEM imaging is highly unreliable owing to artefacts (e. g. particle movement) arising during sample drying. Hence, Fig. 3 shows the DLS size distributions (by number) of the ceria nanoparticles dispersed in the different media. The full DLS dataset including zeta potential data is available in the SI in section S3, Figs. S3.4–S3.7. Generally, both ceria nanoparticle morphologies were relatively well dispersed in both CCB (at pH values 3.0, 4.0, 5.0 and 6.0) and GLY pH 3.0, although this varied between media. As can be observed, the NPs in

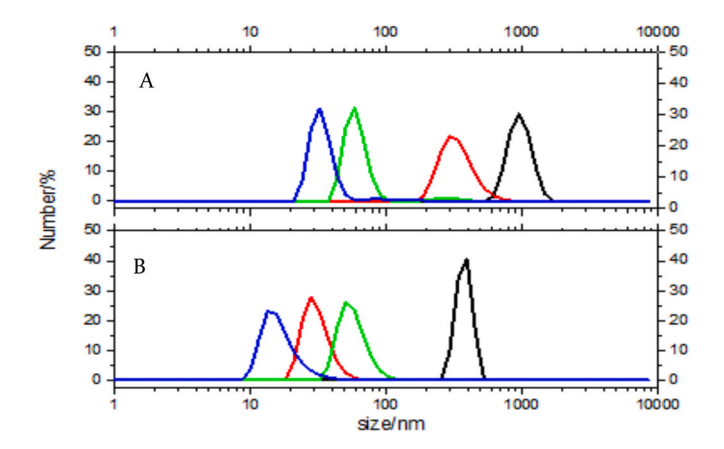


Fig. 3. DLS curves of: (A) Spheres. Black line: in PBS at pH 7.4, red line: in CCB at pH 6.0, green line: in CCB at pH 3.0 and, blue line: in GLY at pH3.0. (B) Cubes: Black line: in PBS at pH 7.4, red line: in CCB at pH 6.0, green line: in CCB at pH 3.0 and, blue line: in GLY at pH3.0.

GLY exhibited the lowest agglomerate size while the NPs in PBS exhibited the largest agglomerate size. The latter could be due to the increase in ionic strength arising from the salts dissolved in the PBS [53,54]. The spheres dispersed in CCB at pH 3.0 exhibited a lower agglomerate size than those dispersed in CCB at pH 6.0, whilst the opposite behaviour was observed for the cubes.

The isoelectric point (IEP) of CeO_2 NPs according to previous studies lies between 5 and 8 [55–62]. Our determination of the IEP of washed, uncoated ceria spheres in water gave a value of 5.75, which is within this range (see SI section S3, Fig. S3.8). Table 1 displays the ZP values of the NPs dispersed in the different media.

NPs dispersed in PBS at pH 7.4 had a negative ZP, which could either be a result of being above the IEP or could arise from adsorption of negatively charged phosphate ions in the buffer. CeO_2 NPs dispersed in CCB at pH 6.0 and 3.0 both had negative ZP values despite being close to or below the IEP, respectively. Presumably, the behaviour arises due to the absorption of negatively charged citrate ions onto the positively charged CeO_2 NPs. Finally, CeO_2 NPs in GLY at pH 3.0 exhibited highly positive ZP values in accordance with the low agglomerate size observed by DLS. At that pH, glycine is expected to be neutral (pKa₁ = 2.4 [43,63]). However, this behaviour is presumably caused due to the excess of H^+ from the HCl of the buffer in solution.

3.2. Electrochemical measurements

3.2.1. Stability of the DOPC layer on a Hg/Pt electrode under different conditions

The behaviour of the phospholipids on the electrode depends on its polar heads. Therefore, the dispersion medium, which is in contact with

Table 1Zeta potential values of ceria spheres and cubes in different media.

| | | Spheres | Cubes |
|-------|-----|---------------|-----------|
| Media | pН | ZP (mV) | ZP (mV) |
| PBS | 7.4 | -17.4 ± 0.6 | -19 ± 1 |
| CCB | 6.0 | -22 ± 1 | -22 ± 1 |
| CCB | 3.0 | -21.5 ± 0.6 | -22 ± 1 |
| GLY | 3.0 | 33 ± 3 | 33 ± 2 |

the layer, could alter its stability. Changes in pH marginally affects the polarity of the phospholipid heads. In addition, contaminants and certain components of commercial buffers can directly interact with the phospholipid layer. Consequently, the stability of the DOPC layer in the various dispersion media was confirmed prior to experiments.

DOPC stability on Hg/Pt was assessed by analysing the variation of the voltammogram current peaks with time for the different experimental conditions (Fig. 4). Small periodic changes in current can be produced as a result of instrumental errors and the error of the measurement for each experimental condition was calculated by using the standard deviation of the variation of the current peaks with time. Peak suppression was relatively constant with time which confirmed that the DOPC layer was sufficiently stable under flow to carry out the subsequent experiments. The main criterion for the monolayer stability with flow of buffer is the lack of a peak suppression of more than 20 % over 225 s. This more or less even suppression with time can be related to the interaction of trace contaminants in the buffer with the monolayer and can be used as a control for subsequent experiments.

3.2.2. Analysis of the interactions of the synthesis reactants in their respective media with DOPC using RCV

This high-throughput technique is very sensitive. It has been shown to be able to detect traces of dissolved materials in water [10]. For this reason, it is necessary to evaluate the interaction of any possible contaminant with DOPC so as to avoid false positive results. Fig. 5A–C shows the interaction of 40 mM of TMAOH, 0.5 M of HMT and 39.5 mM of $Ce(NO_3)_3 \cdot 6H_2O$, with DOPC under a continuous flow of PBS.

As observed in Fig. 5A–B, there was no suppression of the current peaks for TMAOH and HMT. This indicates that these reactants, at the synthesis concentrations employed, do not produce an interaction with DOPC. However, a distinct peak shift and suppression were seen for Ce (NO₃)₃·6H₂O when it interacted with DOPC in a constant flow of PBS, CCB 3.0 and also GLY 3.0 (Fig. 5C–E respectively); the first peak shifts to lower (less negative) voltages in both PBS and GLY 3.0, whilst the second peak shifts to higher (more negative) voltages in PBS, CCB 3.0 and GLY 3.0. This behaviour suggests a binding between free or complexed Ce(+III) ions and the polar phosphate groups of the phospholipid heads. The polar heads are implicitly involved in the two phase transitions, so an alteration in their conformation and charge will affect the nature of the capacitance current peaks representing the phase transitions.

This interaction additionally highlights the importance of thoroughly removing (by repeated washing, centrifuging and resuspension – as outlined in section 2.2) any unreacted cerium nitrate precursor from the synthesised ceria nanoparticle samples.

3.2.3. The role of media in the interaction of CeO₂ NPs with DOPC Fig. 6 displays the RCV profiles of DOPC when in contact with CeO₂

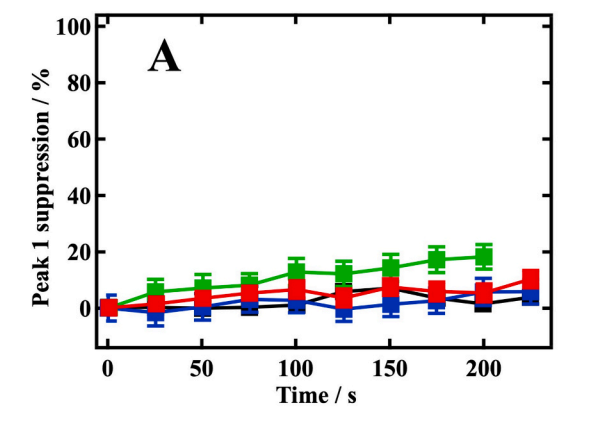
NPs in different media. Fig. 6A–D corresponds to 0.01 M CeO $_2$ NP spheres in PBS at pH 7.4, CCB at pH 6.0, CCB at pH 3.0 and GLY at pH 3.0, respectively. Meanwhile Fig. 6E–H corresponds to 0.01 M CeO $_2$ NP cubes in PBS at pH 7.4, CCB at pH 6.0, CCB at pH 3.0 and GLY at pH 3.0, respectively.

As observed in Fig. 6, the suppression of the current peaks increased as the pH decreased. Neither spheres nor cubes produced an interaction with DOPC at pH 7.4 (PBS) and pH 6.0 (CCB) (A, B, E and F in Fig. 6). Similar behaviour was observed for ceria spheres and cubes in CCB at pH values of 4.0 and 5.0 (data shown in the SI section S4, Figs. S4.1 and S4.2). However, in CCB at pH 3.0 (C and G in Fig. 6), a decrease in the current peaks and a distinct shift of the second peak (to more negative voltages) were produced for the case of both ceria spheres and ceria cubes. The peak shift was more pronounced in the second peak, which corresponds to a DOPC bilayer with patches [15,46]. In addition, a clear increase in the background current (a so-called semiconductor effect) was observed in the region -1.1 V to -1.2 V, which indicates the samples had direct access to patches of uncoated Hg/Pt electrode [15].

Fig. 6D and H show the interaction of spheres and cubes, respectively, with DOPC under a continuous flow of GLY at pH 3.0. A suppression and distinct shift of both peaks were observed for both nanoparticle types. This suggests that the sample interacts directly with the polar heads of the phospholipids, changing the polarity of the layer, leading to a peak shift, and hampering the passage of ions and water, which generates a decrease of the current. In addition, a background current increase in the region $-1.1~\rm V$ to $-1.2~\rm V$ was again observed, which indicates the samples go through the perturbed phospholipid layer and interact directly with the uncoated Hg/Pt electrode.

Firstly, the observed nanoparticle-membrane interactions measured by RCV do not seem to be a function of agglomerate size in the different media, as both types of ceria NPs in CCB pH 3.0, CCB pH 4.0, CCB pH 5.0, CCB pH 6.0 and also GLY pH 3.0 were all relatively well dispersed (see the SI section S3, Figs. S3.4–S3.7). Furthermore, the commercial ceria NPs in PBS pH 7.4 were monodispersed and showed no interaction, although potentially they could be coated.

Secondly, this interaction of the ceria NPs with DOPC in the various media may be directly compared with that produced by free Ce^{3+} ions in the same media (Fig. 5C–E). Ceria NPs in PBS at pH 7.4 (Fig. 6A and E) do not show any interaction, unlike the case of free Ce^{3+} ions (Fig. 5C). However, although ceria NPs in CCB pH 3.0 (Fig. 6C and G) showed a similar effect to that of free Ce^{3+} ions, in terms of the shift of the second capacitance peak, there was no significant increase in background current (Fig. 5D). Similarly, ceria NPs in GLY pH 3.0 (Fig. 6D and H) showed a similar effect to that of free Ce^{3+} ions, in terms of the shifts of both capacitance peaks and particularly the shift of the first peak to lower (less negative) voltages, but again there was no significant increase in background current (Fig. 5E). This could suggest the presence of free



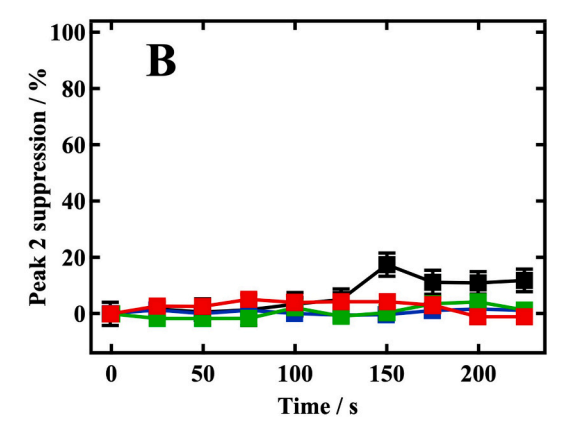


Fig. 4. (A) DOPC peak 1 reduction with time under a continuous flow of: PBS at pH 7.4 (black), CCB at pH 6.0 (red), CCB at pH 3.0 (green) and GLY at pH 3.0 (blue). (B) DOPC peak 2 reduction with time under a continuous flow of: PBS at pH 7.4 (black), CCB at pH 6.0 (red), CCB at pH 3.0 (green) and GLY at pH 3.0 (blue).

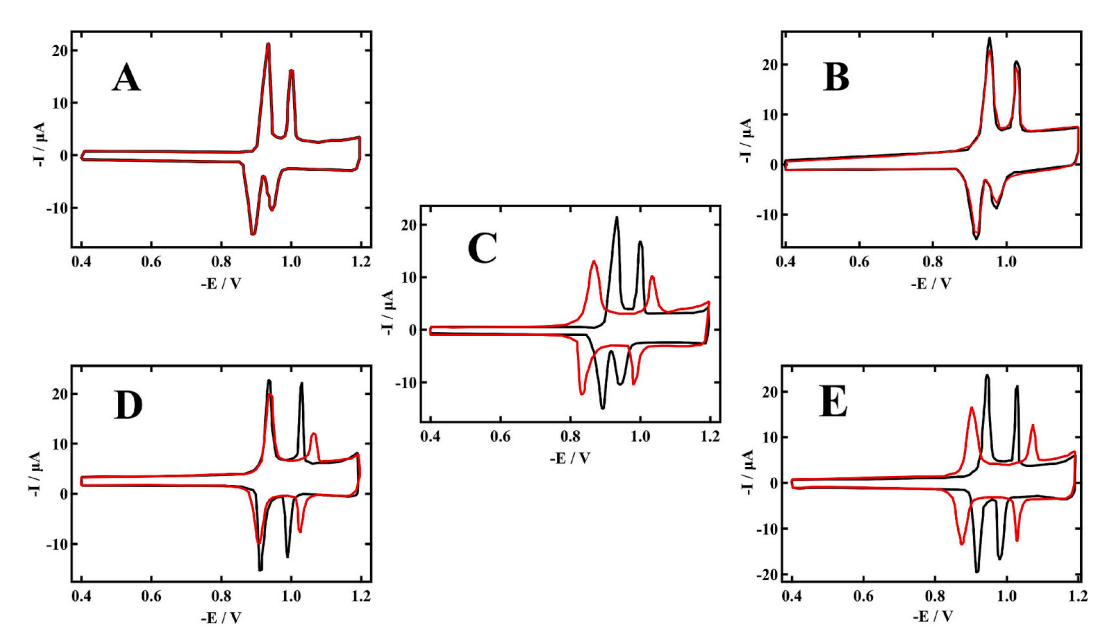


Fig. 5. RCVs recorded at 40 V s⁻¹ from -0.4 V to -1.2 V for DOPC in: (A, B and C) PBS pH 7.4 (black lines); (D) CCB pH 3.0 (black line) and (E) GLY pH 3.0 (black line); and then after adding to PBS pH 7.4: (A) 40 mM TMAOH (red line), (B) 0.5 M of HMT (red line) and (C) 39.5 mM of Ce(NO₃)₃ solution (red line); and after adding 39.5 mM of Ce(NO₃)₃ solution to (D) CCB pH 3.0 (red line) and (E) GLY pH 3.0 (red line).

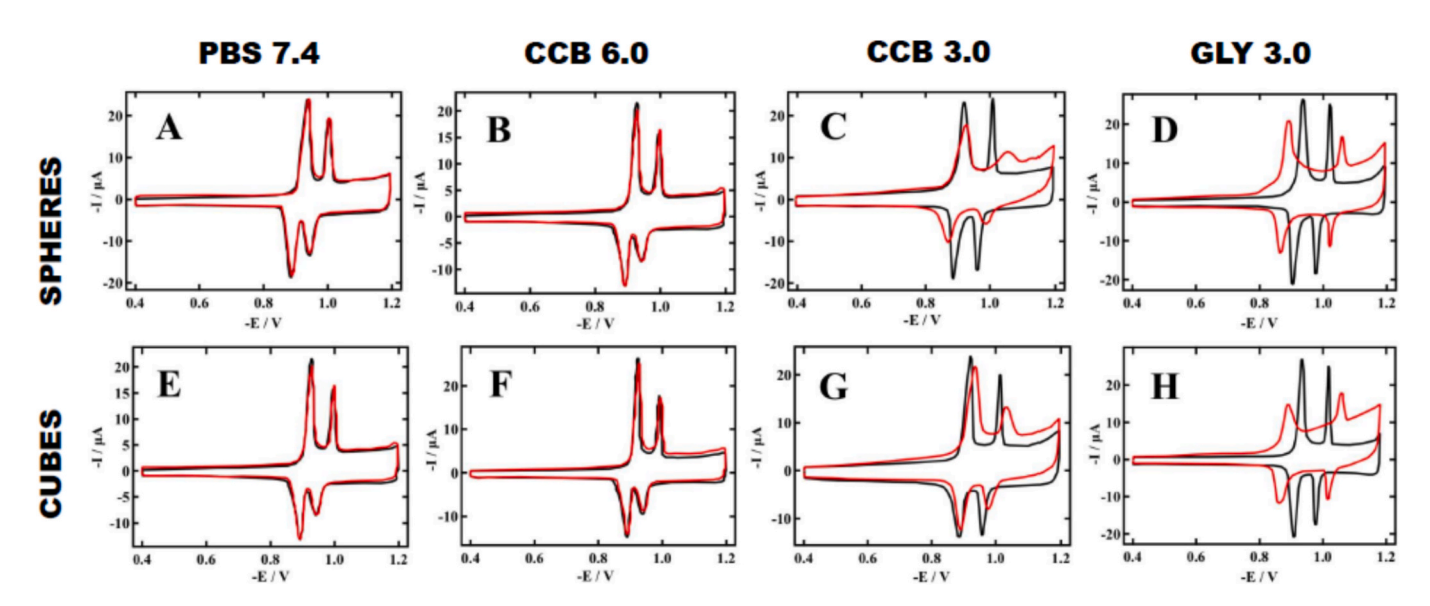


Fig. 6. RCVs recorded at 40 V s⁻¹, with excursions from -0.4 to -1.2 V, of DOPC and DOPC exposed to 0.01 mol dm⁻³ Ce as CeO₂ particles: (A) DOPC in PBS pH 7.4 (black line) plus spheres (red line); (B) DOPC in CCB pH 6.0. (black line) plus spheres (red line); (C) DOPC in CCB pH 3.0 (black line) plus spheres (red line); (D) DOPC in GLY pH 3.0 (black line) plus spheres (red line); (E) DOPC in PBS pH 7.4 (black line) plus cubes (red line); (F) DOPC in CCB pH 6.0 (black line) plus cubes (red line); (G) DOPC in CCB pH 3.0 (black line) plus cubes (red line); (H) DOPC in GLY pH 3.0 (black line) plus cubes (red line).

Ce³⁺ ions in the CCB pH 3.0 and GLY pH 3.0 ceria NP samples at this acidic pH. However, in both cases, the peak shifts and suppressions were also accompanied by the semiconductor effect (the background current increase at high voltages), which may suggest the direct interaction of the ceria NPs with the uncoated Hg/Pt electrode.

For the case of ceria NPS in CCB, the observed RCV responses can be explained by the fact that citric acid (H₃CA) is a triprotic acid with three pK_a values: 3.13, 4.76, and 6.40 at 25 °C. As a result, at pH values of 3 and 6, the ratios of [H₃CA]/([H₂CA $^-$] + [H₃CA]) and [HCA $^2^-$]/([CA $^3^-$ + HCA $^2^-$]) are \sim 57 % and \sim 72 % respectively. This means that the average negative charge numbers of citric acid at pH 3 and pH 6 are 0.43 and 2.58 respectively. As a result, the citrate ion has six times the capacity to complex Ce(III) at pH 6, than it has at pH 3 which clarifies why

any Ce(III) species are relatively uncomplexed with citrate at the lower nH.

3.2.4. Dissolution of ceria nanoparticles and the potential presence of Ce^{3+} ions in solution

Ceria is often reported as being insoluble under normal environments, however, studies have suggested CeO_2 NPs may dissolve under acidic conditions [64,65] as indicated by its Pourbaix diagram. Yu et al. [66] indicate that the pH below which Ce (+III) is expected to be stable depends on oxygen partial pressure, and for 0.01 M ceria to produce the dissolution of $> 10^{-6}$ M [Ce^{3+}] ions, the pH must lie somewhere between 3 and 4. Dissolution presumably occurs via a two stage process involving, firstly, the reduction of cerium (+IV) ions at the surface of ceria

nanoparticles to form Ce (+III) species. Secondly, these Ce (+III) species could then, form free (albeit hydrated) Ce^{3+} ions or complexes either at the nanoparticle surface or in solution. Depending on pH, citrate is known to form complexes with Ce^{3+} [67], as is possibly glycine [68].

Thus, the observed RCV results, could arise by one of a number of mechanisms: firstly, the interaction of the phospholipid membrane with reduced Ce(+III) species at the ceria nanoparticle surface; secondly, the interaction of complexed Ce(+III) species at the ceria nanoparticle surface; thirdly the direct interaction with free (hydrated) or complexed Ce^{3+} ions in solution and; finally, a combination of these three mechanisms.

However, there is no clear agreement about the presence of reduced Ce³⁺ on the surface of ceria particles as the result depends sensitively on the measurement technique that it is used (e.g. whether the sample is analysed in a vacuum or a hydrated atmosphere, etc.) [69-74]. We attempted analyses of the valence state of the ceria nanoparticle samples following 30-minute exposure to the different media using TEM/EELS measurements of the cerium M_{4.5}-edges [75,76]. CeO₂ NPs (spheres) were dispersed in GLY 3.0, CCB 3.0 and PBS 7.4 and drop-cast onto holey carbon-coated TEM grids and allowed to dry. EELS spectra, from five different areas (approximately 150 nm in diameter) were taken to study the Ce³⁺/Ce⁴⁺ ratio produced in different media. Fig. S5.1 in section S5 of the SI displays the EELS spectra of the spheres in different media. The Ce³⁺/Ce⁴⁺ ratio on the particle surface was calculated by non-linear least squares fitting of the cerium M₅ and M₄ "white line" peaks of the sample spectra with those from Ce⁴⁺ and Ce³⁺ reference materials (commercial cerium (IV) oxide nanoparticles and cerium (III) phosphate, respectively). The $\text{Ce}^{3+}/\text{Ce}^{4+}$ ratio was found to be 0.03 ± 0.02 in PBS, 0.02 ± 0.01 in CCB 3.0 and 0.11 ± 0.08 in GLY 3.0. Spheres in PBS and CCB 3.0, therefore, do not appear to have any significant Ce³⁺ on their surface. However, spheres in GLY 3.0 present a relevant amount (ca. 11 %) of Ce³⁺ as evidenced by a slight shift of both cerium M₅ and M₄ "white line" peaks to lower energy loss (relative to the Ce⁴⁺ reference) and a small change in the M_{5/}M₄ white line intensity ratio, indicative of the presence of Ce³⁺ potentially on the particle surface. For a particle 3 to 4 nm in diameter, the approximate amount of cerium atoms on the NP surface can be estimated to be around 30 %, thus this result implies that approximately a third of the cerium atoms on the NPs in GLY 3.0 could be Ce³⁺ if the defects were all located on the NP surface. However, we note that the uncertainties in the measured values are relatively large and that the sample has been dried for TEM analysis and measured under vacuum. Furthermore, the sample preparation route involved drying a drop of the dispersion on the TEM grid and thus, potentially the measurement could also include any dried dissolved (or complexed) Ce³⁺ in solution, or that drying could even lead to the removal of any weakly bound Ce³⁺ complex on the surface of the ceria nanoparticles.

In terms of the presence of soluble Ce³⁺ ions or complexes produced from dissolution of the CeO2 NPs in the different media, many reports in the literature have been undertaken using ICP-MS and have involved separation of the particulate material from the supernatant by simple centrifugation, which does not necessarily guarantee small NPs are not present in the liquid phase which is most often acid digested before subsequent ICP-MS analysis [45]. We have conducted our own dissolution experiments using ICP-MS following the centrifugationultrafiltration procedure described in [45], and hence, the results should accurately reflect both free cerium ions and/or complexes in solution. Table 2 shows the amount of dissolved cerium measured by ICP-MS, which is produced when 0.01 M concentrations of spheres and cubes were dispersed in GLY, CCB and PBS (pH values 3.0, 3.0 and 7.4, respectively) for 30 min. In PBS at pH 7.4 and GLY 3.0 there is no firm evidence for any significant dissolution of ceria NPs, whilst in CCB 3.0 there could be evidence for a small, yet potentially significant, concentration of Ce(III) in the media which could possibly exist as a weak complex with citrate ions. We appreciate the centrifugation step could have potentially detached any weakly bound complexes from the surface

Table 2ICP-MS Determination of the amount of elemental cerium obtained after dispersing spheres and cubes in different media and pH.

| Sample | Medium | pН | [Ce] _{dis} (%) | [Ce] _{dis} (M) |
|---------|--------|-----|-------------------------|-------------------------|
| Spheres | GLY | 3.0 | 0.03 | 3×10^{-6} |
| | CCB | 3.0 | 0.27 | $3	imes10^{-5}$ |
| | PBS | 7.4 | 0.01 | $1 	imes 10^{-6}$ |
| | | | | |
| Cubes | GLY | 3.0 | 0.03 | 3×10^{-6} |
| | CCB | 3.0 | 0.05 | $5 	imes 10^{-6}$ |
| | PBS | 7.4 | 0.02 | 2×10^{-6} |

of the nanoparticles. Similar results were obtained for CCB pH 4.0, CCB pH 5.0 and CCB pH 6.0.

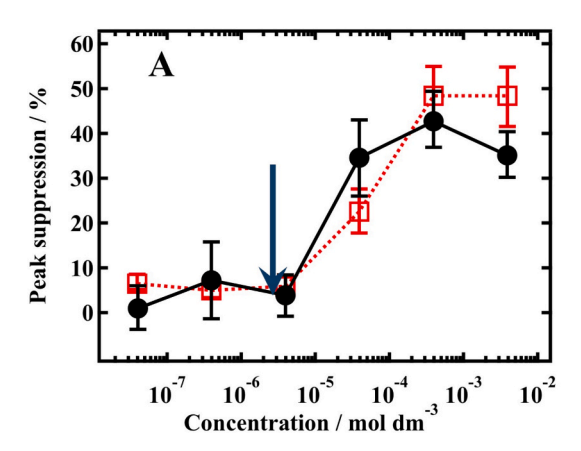
TEM imaging of the average particle sizes of both spheres and cubes after dispersion in the different media suggested a small reduction in particle size for both CCB and GLY buffers relative to PBS at pH 7.4 (see the SI section 5, Table S5.1 and Fig. S5.2). This may suggest some dissolution of nanoparticles when in CCB and GLY, however, differences were relatively small and close to standard deviations of the fitted measurements. Furthermore, any low density, amorphous surface complex may not be easily visible when superimposed on the thin amorphous carbon TEM support film.

3.2.5. Understanding the effect of Ce^{3+} ions on the RCV results

Here we wish to ascertain whether the RCV response to ceria NPs at low pH was due to dissolved cerium ions/complexes in solution. During the methodological development of the research, it was decided not to test directly the RCV response of the supernatant following nanoparticle incubation and separation, as we believed this could have led to a false positive result. This is because that although the centrifugation/ultrafiltration separation procedure described should in principle remove all nanoparticulate matter, owing to the very small size of the nanoparticles (a few nanometres), it is possible that not all the nanoparticles were successfully removed by ultrafiltration and could have contributed to an RCV response. The concentration of soluble cerium ions following nanoparticle incubation as measured by ICP-MS could therefore be a slight overestimate and represents an upper bound. Therefore, as an alternative approach to evaluate how free Ce³⁺ ions affected the phospholipid monolayer, we decided to use soluble cerium nitrate as a source of Ce³⁺ ions.

Fig. 7A and B show RCV measurements of the average peak suppression of the current peaks when DOPC was exposed to different concentrations of Ce(NO₃)₃·6H₂O in GLY 3.0 and CCB 3.0, respectively. The limit of detection (LOD) for Ce³⁺ was found to be 4×10^{-6} M in GLY 3.0 and 4×10^{-5} M in CCB 3.0 respectively. Assuming cerium ion-media complexation reduces or even removes an interaction of Ce³⁺ ions with the membrane (depending on the charge on the specific complex at a given pH), the higher LOD for CCB 3.0 may imply more complexation in CCB 3.0 and more free or hydrated Ce³⁺ ions in GLY 3.0, in agreement with the pK₃ data discussed in section 2.2.1.

In Fig. 7, the vertical blue arrows represent the amount of dissolved Ce $^{3+}$ obtained from the ceria nanoparticle dissolution experiments and ICP-MS analyses when 0.01 M of ceria NPs were dispersed in GLY 3.0 and CCB 3.0 (averaged between spheres and cubes, see Table 2). The results suggest that the concentration of dissolved or complexed Ce $^{3+}$ ions produced when 0.01 M ceria spheres and cubes were dispersed in both GLY 3.0 and CCB 3.0 ((2.9 \pm 0.3)·10 $^{-6}$ M and (2 \pm 1)·10 $^{-5}$ M, respectively) is at or below the LOD for Ce $^{3+}$ ions (from dissolved cerium nitrate) in the same relevant buffer. As discussed above, the fact that we believe that this ICPMS result represents an upper bound for the concentration of dissolved cerium ions following nanoparticle incubation strongly suggests that any observed RCV interaction of ceria nanoparticles observed at low pH is not due to any free or complexed Ce $^{3+}$ ions within the solution. Hence, the magnitude of the peak shifts and



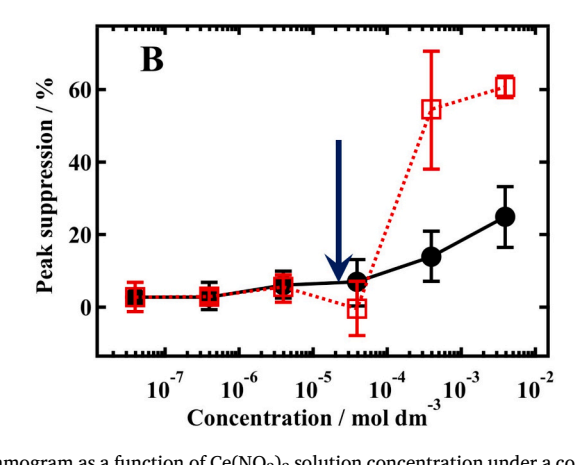


Fig. 7. Suppression of peak 1 (black circles) and peak 2 (red squares) of the voltammogram as a function of Ce(NO₃)₃ solution concentration under a constant flow of: (A) GLY pH 3.0 and, (B) CCB pH 3.0. The average cerium concentration in solution from ICP-MS experiments (displayed by vertical blue arrow) dissolved from 0.01 M of CeO₂ NPs (spheres/cubes) in (A) GLY and (B) CCB pH 3.0.

peak suppressions observed in the RCV profiles in Fig. 6 are most likely due to the direct interaction of the phospholipid monolayer with reduced cerium ions on the surface of ceria nanoparticles. For the case of GLY 3.0, based on pKa values, one would expect these Ce^{3+} ions not to be complexed, whilst for the case of CCB 3.0 there could be some weak complexation or coating (e.g. a "soft" nanoparticle corona) at the reduced ceria nanoparticle surface.

For completeness, Fig. 8(A–C) shows the average peak suppression of the RCV current peaks when DOPC was exposed to varying concentrations of Ce^{3+} from $Ce(NO_3)_3 \cdot 6H_2O$ in CCB at pH 4.0, 5.0 and 6.0, respectively. Here there was no significant peak suppression observed for any level of Ce^{3+} concentration and thus no interaction with the DOPC layer. However, a RCV peak suppression was observed for Ce^{3+} in CCB pH 3.0 (Fig. 7B), which suggests citrate is more strongly complexing with Ce^{3+} ions and hampering their interaction with the phospholipid monolayer at pH values \geq 4. Strong complexation of any reduced cerium ions at ceria nanoparticle surfaces (e.g. a "hard" nanoparticle corona) would then explain the absence of any interaction of ceria nanoparticles with the phospholipid monolayer observed in CCB 6.0 (Fig. 6) and also in CCB 5.0 and CCB 4.0 (see the SI, section S4).

3.2.6. The role of phosphate on ceria nanoparticle interactions with the model membrane

Finally, it has been reported that PBS can coat the surface of CeO_2 NPs and modify their activity [77,78]. To study the effect of PBS in the system under study, 0.01 M of CeO_2 NPs (spheres) were dispersed in PBS for 24 h in order to coat the NPs. The sample was then centrifuged for 30 min at 14000 rpm and the supernatant removed. Subsequently, a certain volume of either CCB at pH 3.0 or GLY at pH 3.0 was added to the dried pellet to maintain the concentration at 0.01 M. Finally, the samples were

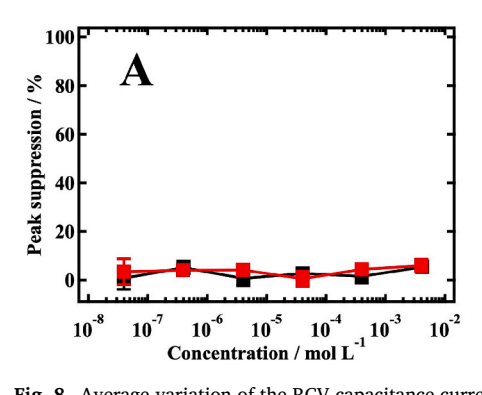
sonicated for 30 min to re-disperse the NPs.

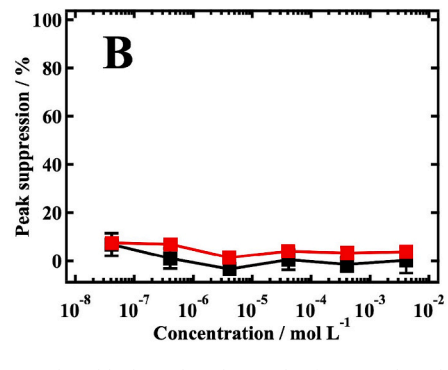
Fig. 9 shows the RCV profiles of the PBS-coated ceria spheres in the different buffers. As observed, a light peak suppression was observed in both cases. Fig. 9A (CCB pH 3.0) displays a decrease in the current of the first and the second peak, whilst Fig. 9B (GLY pH 3.0) shows a decrease in the current of the first peak while the second one remains relatively stable. However, these RCV profiles are significantly different from those obtained when the un-coated NPs were dispersed in CCB or GLY at pH 3.0 (Fig. 6). This behaviour, together with TEM results which suggest little change in particle size (see the SI section 5, Table S5.1 and Fig. S5.2), suggests PBS inhibits the activity of CeO₂ NPs at acidic pH by coating the NPs and possibly preventing their reduction to form Ce³⁺ ions at the nanoparticle surface and/or their dissolution or complexation. Such data indicates that the nanoparticle surface is critical in the interaction with the membrane.

4. Conclusions

We have used an electrochemical sensor and rapid cyclic voltammetry to study the interactions of CeO_2 NPs with model membranes. Many groups have debated the mechanisms of the biological activity action of CeO_2 NPs and have proposed either dissolution, surface charge, or oxygen vacancies as the main reasons to explain their behaviour. This study suggests CeO_2 NPs may be able to exhibit both oxidase and reductase-like behaviour because the bioactivity of CeO_2 NPs behaviour depends on particle surface characteristics. In this way, the dispersion media can induce the formation of oxygen vacancies at the particle surface and coatings can hamper or enhance NPs interactions.

The interactions between CeO $_2$ NPs (spheres with 4.28 \pm 0.28 nm diameter and cubes of 10.57 \pm 0.17 nm side) and DOPC were analysed





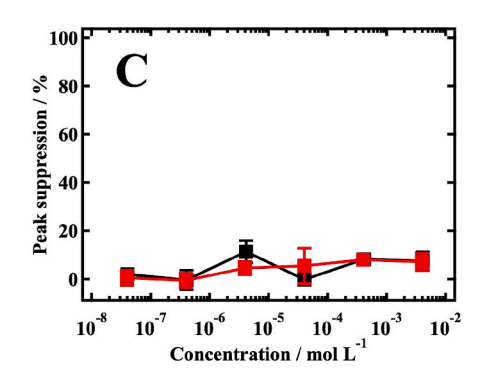


Fig. 8. Average variation of the RCV capacitance current peak 1 (black) and peak 2 (red) of DOPC when the phospholipid is exposed to different concentrations of cerium, from Ce(NO₃)₃·H₂O, in (A) CCB pH 4.0 (B) CCB pH 5.0 and (C) CCB pH 6.0.

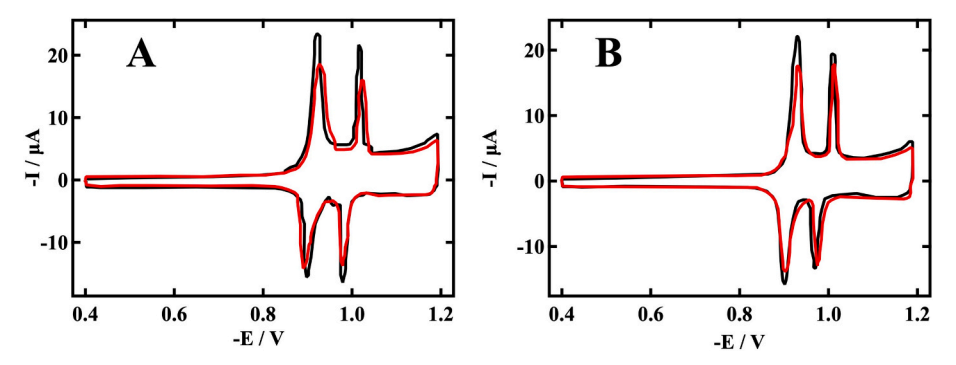


Fig. 9. RCVs recorded at 40Vs^{-1} from -0.4 V to -1.2 V of A: Black line: DOPC under a continuous flow of CCB at pH 3.0, red line: PBS-coated ceria spheres in CCB at pH 3.0. and B: Black line: DOPC under a continuous flow of GLY at pH 3.0 and red line: PBS-coated ceria spheres in GLY at pH 3.0.

using RCV under buffers of different pH (PBS at pH 7.4, CCB at pH 3.0, 4.0, 5.0, 6.0 and GLY at pH 3.0). The agglomeration state of the nanoparticle samples did not appear to correlate with the RCV response; however, the pH of the media did show a distinct correlation. No interaction with DOPC was observed for either spheres or cubes in PBS at pH 7.4 or CCB at pH 4.0, 5.0, or 6.0. However, distinct voltammogram peak suppressions, indicative of different types of interaction with DOPC were present when both NP morphologies were dispersed in GLY and CCB at pH 3.0. The interaction of CeO₂ NPs with DOPC in CCB at pH 3.0 reduced the height and shifted the second peak of the voltammogram to higher potentials. Meanwhile the interaction of CeO₂ NPs with DOPC in GLY at pH 3.0 reduced the height and shifted both the first and second peak of the voltammogram to lower and higher potentials, respectively. Remarkably, these interactions closely resembled those observed for Ce³⁺(aq) ions under equivalent conditions, however this was accompanied by an increase in background current indicative of a direct interaction of the NPs with the model membrane electrode.

Therefore, we attribute the interaction of CeO2 NPs with DOPC in CCB at pH 3.0 to the complexation of Ce(+III) on the particle surface with citrate. At this pH, CCB is known to facilitate the formation of complexes with Ce(+III). For the case of CeO2 NPs interacting with DOPC in GLY at pH 3.0, the observed RCV response is likely to be directly associated with Ce(+III) species at the NP surface. This hypothesis is supported by TEM/EELS measurements, which indicate the presence of significant Ce(+III) on the particle surface when NPs are dispersed in GLY at pH 3.0. However, due to the sample pre-drying and microscope vacuum environment during EELS experiments, which could have induced the formation of oxygen vacancies, this conclusion cannot be unambiguously confirmed. Dissolution experiments were also conducted to investigate whether these observed RCV interactions were instead caused by dissolved Ce³⁺ (aq) ions. The results demonstrated that the concentrations of dissolved cerium ([Ce $^{3+}$]_{GLY3.0} = (2.9 \pm 0.3)· 10^{-6} M and $[Ce^{3+}]_{CCB3.0} = (2 \pm 1) \cdot 10^{-5}$ M respectively) were below the limit of detection of the RCV experiments (LOD(Ce³⁺)_{GLY3.0} = 4×10^{-6} M and LOD(Ce $^{3+}$)_{CCB3.0} = 4 \times 10 $^{-5}$ M respectively), thereby reinforcing the hypothesis that Ce(+III) on the particle surface was responsible for the observed RCV interactions.

The interaction between PBS-coated CeO_2 NPs (spheres) and DOPC in both GLY and CCB at pH 3.0 was also examined. The findings revealed that, unlike uncoated NPs, no notable voltammogram changes were detected. This outcome suggests that the PBS coating impedes the interaction, highlighting the critical role of the NP surface in facilitating model membrane interactions.

Taken together, the present findings suggest the existence of appropriate chemical parameter spaces (based on e.g., pH and/or particle coatings) which can be employed to either enhance or impede the interaction of ceria NPs with membrane systems for either their biomedical use or the prevention of toxicological effects.

CRediT authorship contribution statement

Natalia Domenech-Garcia: Writing – review & editing, Writing – original draft, Methodology, Investigation, Formal analysis, Conceptualization. Nicole Hondow: Writing – review & editing, Supervision, Investigation, Funding acquisition, Formal analysis. Andrew Nelson: Writing – review & editing, Supervision, Project administration, Funding acquisition, Formal analysis, Conceptualization. Rik Drummond-Brydson: Writing – review & editing, Supervision, Project administration, Methodology, Funding acquisition, Formal analysis.

Declaration of competing interest

The authors declare the following financial interests/personal relationships which may be considered as potential competing interests: Natalia Domenech-Garcia, Nicole Hondow, Andrew Nelson and Rik Drummond-Brydson reports financial support was provided by European Union. If there are other authors, they declare that they have no known competing financial interests or personal relationships that could have appeared to influence the work reported in this paper.

Acknowledgement

This work was supported by the EU HORIZON 2020 award HISENTS GA number 685817.

Appendix A. Supplementary data

Supplementary data to this article can be found online at https://doi.org/10.1016/j.apsusc.2025.165007.

Data availability

Data will be made available on request.

References

- P. Falcaro, et al., Application of metal and metal oxide nanoparticles@MOFs, Coord. Chem. Rev. 307 (2016) 237–254.
- [2] X. Luo, et al., Application of nanoparticles in electrochemical sensors and biosensors, Electroanalysis 18 (4) (2006) 319–326.
- [3] A.-H. Lu, E.L. Salabas, F. Schüth, Magnetic nanoparticles: synthesis, protection, functionalization, and application, Angew. Chem. Int. Ed. 46 (8) (2007) 1222–1244.
- [4] D.H. Jo, et al., Size, surface charge, and shape determine therapeutic effects of nanoparticles on brain and retinal diseases, Nanomed. Nanotechnol. Biol. Med. 11 (7) (2015) 1603–1611.
- [5] W.J. Stark, et al., Industrial applications of nanoparticles, Chem. Soc. Rev. 44 (16) (2015) 5793–5805.
- [6] T.A. Kuhlbusch, et al., Nanoparticle exposure at nanotechnology workplaces: a review, Part. Fibre Toxicol. 8 (2011) 22.
- [7] M.L.S. Oliveira, et al., Nanoparticles from construction wastes: a problem to health and the environment, J. Clean. Prod. 219 (2019) 236–243.

- [8] L. Calderón-Garcidueñas, et al., Combustion-derived nanoparticles, the neuroenteric system, cervical vagus, hyperphosphorylated alpha synuclein and tau in young Mexico City residents, Environ. Res. 159 (2017) 186–201.
- [9] Z. Coldrick, et al., High throughput systems for screening biomembrane interactions on fabricated mercury film electrodes, J. Appl. Electrochem. 41 (8) (2011) 939–949.
- [10] S. Mohamadi, et al., Electrochemical screening of biomembrane-active compounds in water, Anal. Chim. Acta 813 (2014) 83–89.
- [11] J. Owen, et al., High-throughput electrochemical sensing platform for screening nanomaterial-biomembrane interactions, Rev. Sci. Instrum. 91 (2) (2020) 025002.
- [12] A. Vakurov, R. Brydson, A. Nelson, Electrochemical modeling of the silica nanoparticle-biomembrane interaction, Langmuir 28 (2) (2012) 1246–1255.
- [13] A. Vakurov, et al., ZnO nanoparticle interactions with phospholipid monolayers, J. Colloid Interface Sci. 404 (2013) 161–168.
- [14] A. Vakurov, et al., Significance of particle size and charge capacity in TiO₂ nanoparticle-lipid interactions, J. Colloid Interface Sci. 473 (2016) 75–83.
- [15] A. Nelson, Electrochemical analysis of a phospholipid phase transition, J. Electroanal. Chem. 601 (2007) 83–93.
- [16] A. Nelson, N. Auffret, J. Borlakoglu, Interaction of hydrophobic organic compounds with mercury adsorbed dioleoylphosphatidylcholine monolayers, Biochim. Biophys. Acta Biomembr. 1021 (2) (1990) 205–216.
- [17] R. Körner, et al., Phase transformations in reduced ceria: Determination by thermal expansion measurements, J. Solid State Chem. 78 (1) (1989) 136–147.
- [18] M.E. Khalifi, F. Picaud, M. Bizi, Electronic and optical properties of CeO₂ from first principles calculations, Anal. Methods 8 (25) (2016) 5045–5052.
- [19] F. Esch, et al., Electron localization determines defect formation on ceria substrates, Science 309 (5735) (2005) 752–755.
- [20] J. Kašpar, P. Fornasiero, M. Graziani, Use of CeO₂-based oxides in the three-way catalysis, Catal. Today 50 (2) (1999) 285–298.
- [21] J. Kašpar, P. Fornasiero, N. Hickey, Automotive catalytic converters: current status and some perspectives, Catal. Today 77 (4) (2003) 419–449.
- [22] M. Shelef, R.W. McCabe, Twenty-five years after introduction of automotive catalysts: what next? Catal. Today 62 (1) (2000) 35–50.
- [23] A. Bueno-López, Diesel soot combustion ceria catalysts, Appl. Catal. B 146 (2014) 1–11.
- [24] M. Mogensen, et al., Physical properties of mixed conductor solid oxide fuel cell anodes of doped CeO2, J. Electrochem. Soc. 141 (8) (1994) 2122–2128.
- [25] G.R. Bamwenda, H. Arakawa, Cerium dioxide as a photocatalyst for water decomposition to O₂ in the presence of Ce⁴⁺ and Fe³⁺ species, J. Mol. Catal. A Chem. 161 (1) (2000) 105–113.
- [26] G.R. Bamwenda, et al., The photocatalytic oxidation of water to O₂ over pure CeO₂, WO₃, and TiO₂ using Fe³⁺ and Ce⁴⁺ as electron acceptors, Appl. Catal. A 205 (1) (2001) 117–128.
- [27] S.H.S. Chan, et al., Recent developments of metal oxide semiconductors as photocatalysts in advanced oxidation processes (AOPs) for treatment of dye wastewater, J. Chem. Technol. Biotechnol. 86 (9) (2011) 1130–1158.
- [28] S.M. Hirst, Anti-inflammatory properties of cerium oxide nanoparticles, Small 5 (2009) 2848–2856.
- [29] W. Lin, Y.H.X. Zhou, et al., Toxicity of cerium oxide nanoparticles in human lung, Cancer Cells 25 (6) (2006) 451–457.
- [30] A. Rocca, et al., Pilot in vivo investigation of cerium oxide nanoparticles as a novel anti-obesity pharmaceutical formulation, Nanomed. Nanotechnol. Biol. Med. 11 (7) (2015) 1725–1734
- [31] J.M. Dowding, et al., Cerium oxide nanoparticles protect against a[beta]-induced mitochondrial fragmentation and neuronal cell death, Cell Death Differ. 21 (10) (2014) 1622–1632.
- [32] C. Korsvik, et al., Superoxide dismutase mimetic properties exhibited by vacancy engineered ceria nanoparticles, Chem. Commun. 10 (2007) 1056–1058.
- [33] I. Celardo, et al., Pharmacological potential of cerium oxide nanoparticles, Nanoscale 3 (4) (2011) 1411–1420.
- [34] C. Xu, X. Qu, Cerium oxide nanoparticle: a remarkably versatile rare earth nanomaterial for biological applications, NPG Asia Mater. 6 (2014) e90.
- [35] E.G. Heckert, et al., The role of cerium redox state in the SOD mimetic activity of nanoceria, Biomaterials 29 (18) (2008) 2705–2709.
- [36] A.S. Karakoti, et al., Nanoceria as antioxidant: synthesis and biomedical applications, JOM 60 (3) (2008) 33–37.
- [37] T. Pirmohamed, et al., Nanoceria exhibit redox state-dependent catalase mimetic activity, Chem. Commun. 46 (16) (2010) 2736–2738.
- [38] A. Asati, et al., Surface-charge-dependent cell localization and cytotoxicity of cerium oxide nanoparticles, ACS Nano 4 (9) (2010) 5321–5331.
- [39] S. Lin, et al., Aspect ratio plays a role in the hazard potential of CeO2 nanoparticles in mouse lung and zebrafish gastrointestinal tract, ACS Nano 8 (5) (2014) 4450–4464.
- [40] H. Zhang, et al., Nano-CeO₂ exhibits adverse effects at environmental relevant concentrations, Environ. Sci. Technol. 45 (8) (2011) 3725–3730.
- [41] M.V.D.Z. Park, et al., The effect of particle size on the cytotoxicity, inflammation, developmental toxicity and genotoxicity of silver nanoparticles, Biomaterials 32 (36) (2011) 9810–9817.
- [42] Puntes. V, B.N., Personal communication 2018/19.
- [43] R.M.C. Dawson, et al., Data for Biochemical Research. 1959: Clarendon Press.
- [44] R.N. Goldberg, N. Kishore, R.M. Lennen, Thermodynamic quantities for the ionization reactions of buffers, J. Phys. Chem. Ref. Data 31 (2) (2002) 231–370.
- [45] T.A. Simoes, et al., Evidence for the dissolution of molybdenum during tribocorrosion of CoCrMo hip implants in the presence of serum protein, Acta Biomater. 45 (2016) 410–418.

- [46] A. Nelson, A. Benton, Phospholipid monolayers at the mercury / water interface, J. Electroanal. Chem. Interfacial Electrochem. 202 (1) (1986) 253–270.
- [47] Z. Coldrick, et al., Phospholipid monolayer coated microfabricated electrodes to model the interaction of molecules with biomembranes, Electrochim. Acta 54 (22) (2009) 4954–4962.
- [48] A. Nelson, Electrochemistry of mercury supported phospholipid monolayers and bilayers, Curr. Opin. Colloid Interface Sci. 15 (6) (2010) 455–466.
- [49] L. Ringstad, et al., An electrochemical study into the interaction between complement-derived peptides and DOPC mono- and bilayers, Langmuir 24 (1) (2008) 208–216.
- [50] S. Zhang, A. Nelson, P.A. Beales, Freezing or wrapping: the role of particle size in the mechanism of nanoparticle-biomembrane interaction, Langmuir 28 (35) (2012) 12831–12837.
- [51] Y. Kohl, et al., Rapid identification of in vitro cell toxicity using an electrochemical membrane screening platform, Bioelectrochemistry 153 (2023) 108467.
- [52] B. Crow, et al., Emerging screening platform characterises aminoquinoline structure–activity relationships with phospholipid layers, Bioelectrochemistry 164 (2025) 108927.
- [53] S.-W. Bian, et al., Aggregation and dissolution of 4 nm ZnO nanoparticles in aqueous environments: influence of pH, ionic strength, size, and adsorption of humic acid, Langmuir 27 (10) (2011) 6059–6068.
- [54] J. Lee, et al., The influence of ionic strength and organic compounds on nanoparticle TiO2 (n-TiO2) aggregation, Chemosphere 154 (2016) 187–193.
- [55] L.A. De Faria, S. Trasatti, The point of zero charge of CeO₂, J. Colloid Interface Sci. 167 (2) (1994) 352–357.
- [56] D. Speed, et al., Physical, chemical, and in vitro toxicological characterization of nanoparticles in chemical mechanical planarization suspensions used in the semiconductor industry: towards environmental health and safety assessments, Environ. Sci. Nano 2 (3) (2015) 227–244.
- [57] X. Liu, et al., Enhanced colloidal stability of CeO₂ nanoparticles by ferrous ions: adsorption, redox reaction, and surface precipitation, Environ. Sci. Technol. 49 (9) (2015) 5476–5483.
- [58] Ö. Tunusoğlu, et al., Surfactant-assisted formation of organophilic CeO₂ nanoparticles, Colloids Surf. A Physicochem. Eng. Asp. 395 (2012) 10–17.
- [59] D. Namjesnik, et al., Application of the surface potential data to elucidate interfacial equilibrium at ceria/aqueous electrolyte interface, Adsorption 22 (4) (2016) 825–837.
- [60] N.C. Nelson, et al., Phosphate modified ceria as a Brønsted acidic/redox multifunctional catalyst, J. Mater. Chem. A 5 (9) (2017) 4455–4466.
- [61] K.M. Buettner, C.I. Rinciog, S.E. Mylon, Aggregation kinetics of cerium oxide nanoparticles in monovalent and divalent electrolytes, Colloids Surf. A Physicochem. Eng. Asp. 366 (1) (2010) 74–79.
- [62] J.J. Gulicovski, I. Bračko, S.K. Milonjić, Morphology and the isoelectric point of nanosized aqueous ceria sols, Mater. Chem. Phys. 148 (3) (2014) 868–873.
- [63] S.S. Budavari, The Merck Index An Encyclopedia of Chemicals, Drugs, and Biologicals. 1996, Whitehouse Station, N.J.: Merck and Co. p. 765.
- [64] T.V. Plakhova, et al., Solubility of nanocrystalline cerium dioxide: experimental data and thermodynamic modeling, J. Phys. Chem. C 120 (39) (2016) 22615–22626.
- [65] S.M. Briffa, et al., Uptake and impacts of polyvinylpyrrolidone (PVP) capped metal oxide nanoparticles on Daphnia magna: role of core composition and acquired corona, Environ. Sci. Nano 5 (7) (2018) 1745–1756.
- [66] P. Yu, et al., The phase stability of cerium species in aqueous systems: II. The systems. Equilibrium considerations and pourbaix diagram calculations, J. Electrochem. Soc. 153 (1) (2006) C74.
- [67] A. Seza Bastug, S. Gokturk, T. Sismanoglu, 1:1 Binary complexes of citric acid with some metal ions: stability and thermodynamic parameters, Rev. Inorg. Chem. 27 (1) (2007) 53–65.
- [68] A.I. Lytkin, et al., Thermodynamics of reactions of complex formation for Ce³⁺ and Er³⁺ ions with glycine in an aqueous solution, Russ. J. Phys. Chem. A 91 (6) (2017) 1021–1025.
- [69] S. Deshpande, et al., Size dependency variation in lattice parameter and valency states in nanocrystalline cerium oxide, Appl. Phys. Lett. 87 (13) (2005) 133113.
- [70] F. Zhang, et al., Cerium oxidation state in ceria nanoparticles studied with X-ray photoelectron spectroscopy and absorption near edge spectroscopy, Surf. Sci. 563 (1) (2004) 74–82.
- [71] E. Paparazzo, On the curve-fitting of XPS Ce(3d) spectra of cerium oxides, Mater. Res. Bull. 46 (2) (2011) 323–326.
- [72] C. Paun, et al., Polyhedral CeO₂ nanoparticles: size-dependent geometrical and electronic structure, J. Phys. Chem. C 116 (13) (2012) 7312–7317.
 [73] J.-D. Cafun, et al., Absence of Ce³⁺ sites in chemically active colloidal ceria
- [73] J.-D. Cafun, et al., Absence of Ce⁹⁺ sites in chemically active colloidal ceria nanoparticles, ACS Nano 7 (12) (2013) 10726–10732.
- [74] B. Goris, et al., Three-dimensional valency mapping in ceria nanocrystals, ACS Nano 8 (10) (2014) 10878–10884.
- [75] B.T. Thole, et al., 3d X-ray-absorption lines and the $3d^94f^{n+1}$ multiplets of the lanthanides, Phys. Rev. B 32 (8) (1985) 5107–5118.
- [76] G. Kaindl, et al., M-edge X-ray absorption spectroscopy of 4f instabilities in rareearth systems (invited), J. Appl. Phys. 55 (6) (1984) 1910–1915.
- [77] Y. Xue, K. Zhou, W. Lei, H. Tan, Q. Luan, X. Yao, The vital role of buffer anions in the antioxidant activity of CeO₂ NANOPARTICLES, Chem. Eur. J. 18 (35) (2012).
- [78] G. Pulido-Reyes, et al., Untangling the biological effects of cerium oxide nanoparticles: the role of surface valence states, Sci. Rep. 5 (2015) 15613.